ACS APPLIED MATERIALS & INTERFACES

Research Article

www.acsami.org

Understanding the Thermal and Mechanical Stabilities of Olivine-Type $LiMPO_4$ (M = Fe, Mn) as Cathode Materials for Rechargeable Lithium Batteries from First Principles

Ying Xie,*[,†] Hai-Tao Yu,[†] Ting-Feng Yi,*[,†,‡] and Yan-Rong Zhu[‡]

[†]Key Laboratory of Functional Inorganic Material Chemistry (Heilongjiang University), Ministry of Education, School of Chemistry and Materials Science, Heilongjiang University, Harbin 150080, PR China

[‡]School of Chemistry and Chemical Engineering, Anhui University of Technology, Maanshan, Anhui 243002, PR China

Supporting Information

ABSTRACT: To elucidate the microscopic origin of the difference behaviors, first-principles calculations were performed to investigate the thermal and mechanical stabilities of Li_xFePO_4 and Li_xMnPO_4. The calculated free energies suggested that $LiFePO_4$ and $LiMnPO_4$ are thermal stable with respect to relevant oxides both in their pristine and fully delithiated states. According to the calculations, it can be identified that the shear deformations are more easier to occur with respect to the volume compressions in Li_xFePO_4 and Li_xMnPO_4, and this phenomenon is related to M−O(I) and M−O(II) bonds. Typically for $MnPO_4$, Li^+ extraction from the host structures further weakens the Mn−O(I) bonds by about 33%, and it thus becomes very brittle. The shear anisotropy (A_G) of $MnPO_4$ is abnormally large and has already reached 19.05 %, which is about 6 times as large as that of $FePO_4$. Therefore, shear deformations and dislocations occur easily in $MnPO_4$. Moreover, as the Mn−O(I) bonds in $MnPO_4$ are mainly spread within the {101} and {$\bar{1}$01} crystal planes, the relevant slip systems thus allow the recombination of bonds at the interfaces, leading to the experimentally observed phase transformation. It can be concluded that mechanical reason will play an important role for the poor cycling performance of $MnPO_4$.

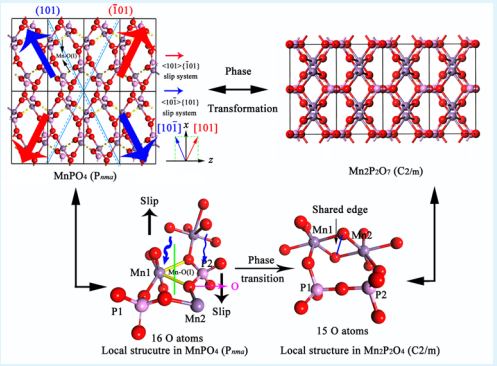

KEYWORDS: *cathode material, lithium iron phosphate, lithium manganese phosphate, thermal stability, mechanical stability*

1. INTRODUCTION

Lithium-ion batteries have continuously gain scientific and commercial concerns in the present age of portable electronics and electric transportation.[1−3] The main efforts are to optimize several factors, including the energy density, rate capability, economy, safety and sustainability.[4,5] To achieve these goals, there have been intensive researches for new materials with promising electrochemical capacity for use as cathodes. Recently, olivine-type $LiMPO_4$ (M = Fe, Mn, Co, and Ni) cathode materials have been proved to be one promising candidate class for lithium-ion batteries due to their low cost, large energy density, and particularly high thermal and electrochemical stabilities.[6−9] However, $LiCoPO_4$ and $LiNiPO_4$ are still difficult to be used in conventional electrolytes at the moment due to the high voltage plateaus close to 4.8[10] and 5.1 V.[11] $LiFePO_4$ and $LiMnPO_4$ offer a moderate redox potential of 3.4 and 4.1 V vs Li^+/Li, which are considered to be the maximum accessible limit to most liquid electrolytes. Therefore, phosphor-olivine-type $LiMPO_4$ (M = Fe, Mn) compounds have attracted much research and technological interests, and many researches are now focused on the olivine $LiFePO_4$ and the more challenging $LiMnPO_4$.[12] But their sluggish kinetics significantly hindered the application. $LiFePO_4$ cathode in principle satisfies the main requirements for a cathode material, but the intrinsically low ionic/electronic conductivity and small tap density were addressed as major problems to be solved before it could be deployed on a commercial scale.[13−15] Previous studies of $LiMnPO_4$ suggested numerous limitations related to its intrinsic electrochemical properties, such as poor electronic conductivity,[16] the instability of $MnPO_4$,[17] the distortion of the Jahn−Teller active Mn^{3+} ion,[18] and the large volumetric change between $LiMnPO_4$ and $MnPO_4$ during charge/discharge processes.[19] Despite of the above pioneer works, however, a clear understanding about the microscopic origin of these effects have not yet been achieved. In the meantime, first principles computation methods have showed superiority in developing and optimizing new energy storage and conversion materials, and the predictions of the material properties are also possible thanks to the density functional theory (DFT).[20,21] To determine some structure-performance relationship of $LiMPO_4$ (M = Fe, Mn), detailed and systematical theoretical investigations are still very urgent.

Received: December 1, 2013
Accepted: March 3, 2014
Published: March 3, 2014

   dx.doi.org/10.1021/am4054833 | ACS Appl. Mater. Interfaces 2014, 6, 4033−4042

Except of the structure−performance relationship, another important criteria for successful implementation of a cathode material is safety, which is usually related to the structural stability of materials. In general, the unstable compounds are easily decomposed due to the thermal reasons. The unstable lattice vibrations (phonons) can also cause a phase transformation, as well known in the soft mode theory. Under external stress, deformations are also available, and the materials would sometimes become mechanically unstable if the condition is appropriate. These factors together govern the structural stability of a compound. In LIBs, it is expected that the host structures of cathode materials should be as stable as possible, because this character may help the cathode to maintain excellent cycling performance and safety. Although it is well known that $LiFePO_4$ and delithiated $FePO_4$ have high thermal stabilities, $MnPO_4$ is believed to be highly unstable. It is reported experimentally that $MnPO_4$ transforms into $Mn_2P_2O_7$ at 120−210 °C with evolution of O_2.[22] But some recent reports argue that no evidence is found that $MnPO_4$ or $[MnFe]PO_4$ have lower thermal stability than $FePO_4$.[23] The exothermal reactivity of de-lithiated olivine phase materials was found to follow the order, $Li_{0.1}MnPO_4$ > $Li_{0.05}Mn_{0.8}Fe_{0.2}PO_4$ > $Li_{0.05}FePO_4$ while using 1 M $LiPF_6$ in EC:DMC as the electrolyte, whereas the above trend was reversed while using 1 M $LiPF_6$ in EC/PC.[23] To clarify the issue, in this paper, it is our target to contribute understanding towards the relationship among geometries, thermal and mechanical stabilities, and bonding characteristics of the compounds, and to discuss the microscopic origin for the different behaviors of Li_xMPO_4 (M = Fe, Mn).

2. THEORETICAL AND COMPUTATIONAL DETAILS

The calculations were performed by means of the CASTEP package in the density functional theory (DFT) framework.[24] The Perdew-Wang generalized gradient approximation form (GGA-PW91)[25] of the exchange correlation energy has been used within its spin-polarized version. To deal with the strong-correlated systems, the Hubbard U parameter was tested as shown in Figure 1, and then introduced in relevant calculations. During the calculations, the plane-wave technique was employed and the energy cutoff was set to 380 eV. To obtain a good numerical sampling of electron densities in Brillouin zone, a Monkhorst-Pack mesh[26] (3 × 4 × 5) was applied. The original valence configurations for the ultrasoft pseudopotentials were $2s^22p^4$ for O, $3s^23p^3$ for P, $3d^54s^2$ for Mn, $3d^64s^2$ for Fe, and $1s^22s^1$ for Li. For the geometry optimization, a Broyden−Fletcher−Goldfarb−Shanno (BFGS) algorithm[27] was used, and the optimization procedure was repeated until the force on each atom was less than 0.05 eV·Å^{-1}. This set of parameters also ensured that the total energy of system can be accurately evaluated, and the energy convergences of systems are within 1.0×10^{-6} eV·atom^{-1}.

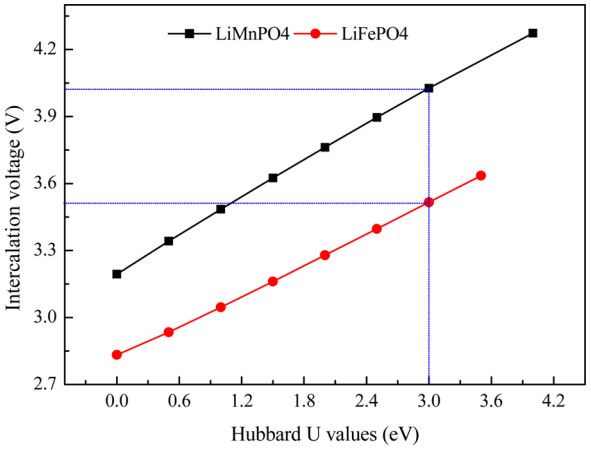

Figure 1. Relationship between intercalation voltage and Hubbard *U* values.

The calculation models for olivine structure $LiFePO_4$ and $LiMnPO_4$ were shown in Figure 2. Their space groups are both

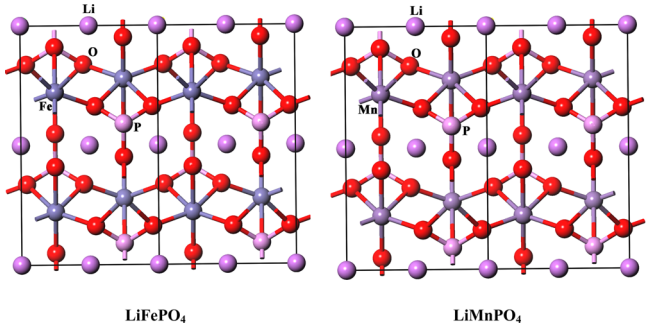

Figure 2. Calculation models for olivine structure $LiFePO_4$ and $LiMnPO_4$.

Pnma containing four formula units. The Li and Fe are located in octahedral sites and P is located in tetrahedral sites with a distorted hexagonal close-packed framework. A MO_6 (M = Fe, Mn) octahedron is edge shared with two LiO_6 octahedrons and one PO_4 tetrahedron, and there is no continuous network of MO_6 (M = Fe, Mn), and the PO_4 tetrahedron is in the middle of the octahedral. Within the crystal structure, there is a one-dimensional tunnel formed by the edge shared LiO_6 octahedrons, and the Li^+ are mobile in this tunnel.

3. RESULTS AND DISCUSSION

3.1. Geometries, Intercalation Voltages, and Thermodynamic Properties. All optimized lattice constants, together with the experimental values taken from refs 28−30 are listed in Table 1.

The differences between calculated and experiments values are found to be small, indicating that the theoretical method applied is moderate. When lithium deintercalates from the cathode, *a* and *b* axes slightly decrease while *c* axis increases, which is consistent with the experimental findings. The volume change of $LiFePO_4$ upon de/lithiation is calculated to be about

Table 1. Optimized Geometries and Intercalation Voltages of Li_xMPO_4 (M = Fe, Mn; *x* = 0, 1)

	a (Å)	*b* (Å)	*c* (Å)	*V* (Å^3)	voltage (vs Li/Li$^+$)
$LiFePO_4$	10.339	6.029	4.725	294.565	3.52[a]
exptl.[28]	10.323	6.005	4.693	290.917	
$FePO_4$	9.949	5.994	4.903	292.387	
exptl.[29]	9.8142	5.7893	4.782	271.982	
$LiMnPO_4$	10.573	6.185	4.784	312.802	4.03[a]
exptl.[30]	10.452	6.105	4.745	302.776	
$MnPO_4$	9.918	6.051	4.927	295.735	
exptl.[30]	9.947	5.918	4.781	281.440	

[a]GGA+U method was applied.

dx.doi.org/10.1021/am4054833 | ACS Appl. Mater. Interfaces 2014, 6, 4033−4042

Table 2. Calculated Formation Enthalpies (in kJ·mol^{-1}) and Gibbs Formation Energies (in kJ·mol^{-1}) of Some Cathode Materials

compounds	$\Delta_f H_{m,el.}$	$\Delta_f G_{m,el.}$[a]	ΔE[b]	$\Delta_r G_{m,ox.}$[c]
$LiFePO_4$	−1682.36	−1569.47		−287.51
$FePO_4$	−1343.13	−1230.24	339.23	−142.05 (206.89)[d]
$LiMnPO_4$	−1835.11	−1722.21		−297.79
$MnPO_4$	−1446.58	−1333.69	388.53	−103.41 (152.34)[d]
$LiCoO_2$	−670.90 (−679.40)[e]	−628.79		−133.54 (−142.54)[e]
CoO_2	−262.28	−238.44	390.35	−24.24
$LiNiO_2$	−587.91 (−593.00)[e]	−541.35		−48.76 (−56.21)[e]
NiO_2	−186.28	−158.02	383.33	53.52
$LiMn_2O_4$	−1380.77 (−1380.90)[e]	−1268.62		−81.87 (−82.47)[e]
Mn_2O_4	−1118.70	−1008.92	249.6	−78.64

[a]Gibbs formation energies from elements. (Elemental phases were taken as reference points.) [b]Changes of Gibbs formation energies from elements due to Li^+ extraction. [c]Gibbs formation energies from oxides. The absolute values correspond to the Gibbs free energies of relevant decomposition reactions (Oxides were taken as reference points.). MO (M_2O_3) is the favorable decomposition product for $LiMPO_4$ (MPO_4). [d]Gibbs free energy for the decomposition reactions, $MPO_4 \rightarrow 0.5\ M_2P_2O_7 + 0.25\ O_2$. [e]Experimental formation enthalpies ($\Delta H_{m,}$) are taken from refs 39−41.

1%, which not only guarantees its good structure stability but is also helpful for improving the cycling reversibility. For $LiMnPO_4$ compound, it exhibits a larger volume change (~6%) between the two-end phases. Although the calculated volume changes for $LiMPO_4$ (M = Fe and Mn) compounds are smaller than the reported experimental values,[30,31] the trend is identical. Meethong et al. suggested that the misfit at the phase boundary between Li-rich and Li-poor phases for $LiMnPO_4$ (~10%) is larger than that for $LiFePO_4$ (~6.6%) because of the Jahn-Teller effect of Mn^{3+} ions.[32]

To obtain the intercalation voltage, a rather crucial quantity for lithium ion batteries, we have performed some relevant calculations. As we know, the electrochemical reaction of $LiMPO_4$ (M = Fe, Mn) cathode can be explained as follows:

$$\mathrm{Li}_{x_2}\mathrm{MPO}_4(s, Pnma) \underset{\text{discharge}}{\overset{\text{charge}}{\rightleftharpoons}} \mathrm{Li}_{x_1}\mathrm{MPO}_4(s, Pnma) + (x_2 - x_1)\mathrm{Li}^+ + (x_2 - x_1)e \quad (1)$$

The open-cell voltage depends on the chemical potential of lithium in a lithium anode and that in an olivine-type lithium phosphate cathode

$$V(x) = -\frac{\mu_{\mathrm{Li}}^{\mathrm{cathode}}(x) - \mu_{\mathrm{Li}}^{\mathrm{Anode}}}{nF} \quad (2)$$

where F is the Faraday constant; $\mu_{\mathrm{Li}}^{\mathrm{cathode}}(x)$ is the chemical potential of Li in the intercalation compounds; $\mu_{\mathrm{Li}}^{\mathrm{Anode}}$ is the chemical potential of metallic Li, and n is the charge (in electrons) transported by lithium through the electrolyte. To obtained the voltage averaged over the charge states between x_1 and x_2, eq 2 can be rewritten as

$$\overline{V} = -\frac{\int_{x_1}^{x_2}(\mu_{\mathrm{Li}}^{\mathrm{cathode}}(x) - \mu_{\mathrm{Li}}^{0})\mathrm{d}x}{(x_2 - x_1)F} = -\frac{\Delta G_r}{(x_2 - x_1)F} \quad (3)$$

Because the entropy change and volume effect of solid materials ($\Delta G_r \equiv \Delta E_r + P\Delta V_r - T\Delta S_r$) are very small and usually can be neglected, the calculations are significantly simplified by further approximations, and ΔG_r thus can be replaced by the change of internal energy (ΔE_r).[33] eq 3 can be rewritten as[33,34]

$$\overline{V}(x) = -\frac{\Delta G_r}{(x_2 - x_1)F} = -\frac{[E(x_2) - E(x_1)] - [(x_2 - x_1)E(\mathrm{Li})]}{(x_2 - x_1)} \quad (4)$$

where $E(x)$ is the total energy of Li_xMPO_4 ($x_2 > x_1$). To obtain the average voltage, the total energy of lithium metal (solid, $Im\bar{3}m$) is needed, and the corresponding total energies and standard state experimental data[35] of other relevant substances can be found in Table S1 of the Supporting Information (SI). According to eq 4, the average intercalation voltages for Li_xFePO_4 and Li_xMnPO_4 are calculated to be 3.52 and 4.03 V at the range of $0 \le x \le 1$, respectively, while the experimental values for $LiFePO_4$ and $LiMnPO_4$ are reported to be about 3.5[36] and 4.1 V.[37] Our calculated values are quite consistent with the experimental ones.

Except of the intercalation voltage, the thermodynamic stability is another very important quantity for the solid state electrode materials. Especially in lithium ion batteries, such a quantity is usually associated with the cycling performance and safety issue.[38] To evaluate the thermodynamic properties of $LiMPO_4$ (M = Fe, Mn) cathode, the Gibbs formation energies ($\Delta_f G_{m,el.}$) from elements and the Gibbs formation energies ($\Delta_r G_{m,ox.}$) from oxides were calculated. The thermodynamic reactions and computational algorithms are given in detail in SI. Table 2 listed the calculated enthalpies and free energies of some cathode materials. It can be found that the Gibbs formation energies of $LiFePO_4$ and $LiMnPO_4$ from element phases are calculated to be −1569.47 and −1722.21 kJ·mol^{-1}, respectively. The Gibbs formation energy of $LiMn_2O_4$ from elements (−1268.62 kJ·mol^{-1}) is also very negative. For $LiCoO_2$ and $LiNiO_2$, their Gibbs formation energies from elements are much less exothermic. The result seems suggest that $LiFePO_4$, $LiMnPO_4$, and $LiMn_2O_4$ are much more thermodynamically stable than $LiCoO_2$ and $LiNiO_2$. However, Ong and Ceder have proposed a theoretical method to investigate the full thermodynamic phase diagram of some cathode materials, and it is pointed out that a negative formation energies relative to elemental phases is not sufficient to prove that a material is thermodynamically stable,[42,43] because the cathode materials may decompose into oxides rather than the element phases during the working process. In this circumstance, the reaction free energies of relevant decomposition reactions (Gibbs formation energy from oxides) are more reasonable and preferred.

The Gibbs formation energies of the cathode materials from oxides ($\Delta_r G_{m,ox.}$), defined as the free energies that are released when the oxides react to form corresponding cathode materials, were also listed in Table 2. For $LiFePO_4$ and $LiMnPO_4$, the Gibbs formation energies from oxides are −287.51 and −297.79 kJ·mol^{-1} respectively, which are much less exothermic than their values from elements ($\Delta_f G_{m,el.}$). This result suggested that $LiFePO_4$ and $LiMnPO_4$ are hard to decompose into element phases, while they can decompose into relevant oxides much easier during the charge/discharge process. For $LiCoO_2$, $LiNiO_2$, and $LiMn_2O_4$ compounds, the values from oxides are −133.54, −48.76, and −81.87 kJ·mol^{-1}, respectively. The result identified that $LiMn_2O_4$ is less thermodynamically stable with respect to its corresponding oxides than $LiCoO_2$, although it has a much negative Gibbs formation energy from elements. Furthermore, as the Gibbs formation energies of $LiFePO_4$ and $LiMnPO_4$ from oxides are more exothermic than those of $LiCoO_2$, $LiNiO_2$, and $LiMn_2O_4$, it can be deduced that $LiFePO_4$ and $LiMnPO_4$ are more thermodynamically stable with respect to their oxides than $LiCoO_2$, $LiNiO_2$, and $LiMn_2O_4$ compounds.

During the charging process, Li^+ will deintercalate from the cathode, while the electrons will transfer through the external circuit to the anode. The structural changes in cathode materials lead to variable thermodynamics properties. According to similar algorithms, the Gibbs formation energies of $FePO_4$ (*Pnma*) and $MnPO_4$ (*Pnma*) from elements were calculated to be −1230.24 and −1333.69 kJ·mol^{-1}, respectively. In comparison to $LiFePO_4$ and $LiMnPO_4$, the calculated Gibbs formation energies from elements increase respectively by about 339.230 and 388.527 kJ·mol^{-1}. Such differences are also found in $LiCoO_2$, $LiNiO_2$, and $LiMn_2O_4$ compounds and mainly originated from the chemical bonds between Li and O ions. For the Li_2O pure ionic compound, the Gibbs formation energies is −562.104 kJ·mol^{-1},[35] and the bond energy of one pure Li−O ionic bond is thus about −281.052 kJ·mol^{-1}. In $LiMPO_4$ compounds, lithium ions are six coordinated with O (LiO_6 octahedron), while they are four coordinated with O (LiO_4 tetrahedron) in Li_2O. Therefore, it is not difficult to image that the Gibbs formation energy change of MPO_4 from elements with respect to $LiMPO_4$ is slightly larger than the bond energy of pure Li−O ionic bond. And lithium should exist in $LiMPO_4$ compounds as pure ions.

Furthermore, it should be noted that Li^+ extraction from the host structure can also lead to an increase of the Gibbs formation energies from oxides. For $FePO_4$ and $MnPO_4$, the values have increased by about 145.46 and 194.38 kJ·mol^{-1}, but they can remain much negative. Therefore, $FePO_4$ and $MnPO_4$ are still thermodynamically stable with respect to their oxides. However, the situations in CoO_2 and NiO_2 compounds are different. The Gibbs formation energy of CoO_2 ($R\bar{3}m$) from oxide (−24.24 kJ·mol^{-1}) is very close to zero, while the value (53.52 kJ·mol^{-1}) for NiO_2 ($R\bar{3}m$) has already become positive. The results indicated that layered CoO_2 ($R\bar{3}m$) is relatively unstable with respect to relevant oxides, while NiO_2 ($R\bar{3}m$) will decompose into nickel oxide ($Fm\bar{3}m$) spontaneously. As a result, oxygen evolution in the two compounds can be anticipated, as it has been often observed in experiments.[44] Our calculated Gibbs free energies of relevant decomposition reactions confirmed that the thermodynamic stabilities of $LiMPO_4$ and MPO_4 (M = Fe, Mn) relative to their oxide forms are good. It can be expected that their cycling performances would be also good, and they may be suitable for high safety battery applications.

Experimentally, it has already been confirmed that $LiFePO_4$ and $FePO_4$ have high thermal stabilities and they also exhibit excellent cycling stabilities.[31] For $LiMnPO_4$ and its derivatives, there are still some controversies. It is reported that $FePO_4$ is stable up to 500−600 °C in air without losing oxygen,[45] and it is once believed that the charged $MnPO_4$ compound would match the excellent thermal stability of $FePO_4$. However, some recent investigations have cast doubt on this assumption by demonstrating the decomposition of $MnPO_4$ into $Mn_2P_2O_7$ at 120−210 °C with evolution of O_2.[38,46] This seems in stark contrast to $FePO_4$, and oxygen evolution during decomposition at elevated temperatures would limit the use of $LiMnPO_4$ as a cathode because it raises critical safety problems. However, relying on differential scanning calorimetry (DSC), thermogravimetric analysis coupled with mass spectrometry (TGA-MS), powder X-ray diffraction (XRD), and high-resolution scanning electron microscopy (HRSEM) techniques, Martha and coworkers have performed comparative studies of pristine $LiMPO_4$ (M = Fe, Mn, $Mn_{0.8}Fe_{0.2}$), $LCoO_2$, $LiNi_{0.8}Co_{0.15}Al_{0.05}O_2$, and their electrochemically delithiated counterparts before and after heating to 400 °C, and they could not find pronounced differences in the thermal behavior of $LiFePO_4$ and $LiMnPO_4$ compounds at both fully lithiated and delithiated states.[47] They suggested that $LiFePO_4$ and $LiMnPO_4$ cathode materials have comparable thermal stability in their pristine and fully delithiated states, and no evidence is found that $MnPO_4$ or $[MnFe]PO_4$ have lower thermal stability than $FePO_4$.[47]

Although the Gibbs formation energies of MPO_4 (M = Fe, Mn) from oxides are very close and both negative, the phase transformation for $MnPO_4$ is indeed observed in experiments.[38] To provide some relevant information, the reaction free energies for the decomposition pathways, $MPO_4 \rightarrow 0.5\ M_2P_2O_7 + 0.25\ O_2$, were also calculated (Table 2 and Table S2 of SI). The result indicated that the decomposition reaction from $MnPO_4$ to $Mn_2P_2O_7$ is endothermic (152.34 kJ·mol^{-1}), and the counterpart reaction for $FePO_4$ compound (206.89 kJ·mol^{-1}) is more difficult to occur, which is well consistent with experimental findings. It should be noted that except of the thermodynamic reasons, there are still some other possibilities that can cause a phase transition. Especially in lithium ion batteries, the repeated intercalation or deinterclation of Li^+ from the cathode usually result in local stress and strain within the interior of the crystal particles. Excellent reversibility requires that the cathode materials can sustain good structures at specific deformation and remain mechanically stable under stress. To investigate the mechanical behaviors of the two end structures, we have performed some calculations, as discussed below.

3.2. Mechanical Properties of $LiMPO_4$ and MPO_4 (M = Fe, Mn) Compounds. The mechanical response of an electrode material to the stress fields intimately depends on the material's intrinsic elastic properties. When the cathode materials became mechanically unstable under deformations, phase transition may occur, leading to the degradation of the batteries. Therefore, it can be anticipated that there is an important relationship between the mechanical stability and cycling performance during the charge−discharge process. To obtain the knowledge of elastic properties, the elastic stiffness (C_{ij}) and compliance (S_{ij}) constants should be calculated first. The algorithm for calculating the mechanical properties is

Table 3. Calculated Elastic Constants (in GPa) of Li_xMPO_4 (M = Fe, Mn; x = 0, 1) Compounds

	C_{11}	C_{12}	C_{13}	C_{22}	C_{23}	C_{33}	C_{44}	C_{55}	C_{66}
$LiFePO_4$	140.22	69.87	58.84	187.40	49.76	174.16	39.04	45.70	44.99
ref 51	138.90	72.80	52.50	198.00	45.80	173.00	36.80	50.60	47.60
$FePO_4$	182.38	27.62	66.65	115.53	13.34	131.60	31.49	48.26	44.15
ref 51	175.90	29.60	54.00	153.60	19.60	135.00	38.80	47.50	55.60
$LiMnPO_4$	127.49	68.87	48.24	156.73	42.60	151.16	32.82	37.24	39.52
$MnPO_4$	99.62	-36.09	21.19	166.07	−10.60	73.57	16.96	48.71	17.93

Table 4. Bulk Modulus (B, in GPa), Shear Modulus (G, in GPa), Young's Modulus (E, in GPa), and Poisson's Ratio (ν) for Polycrystalline Li_xMPO_4 (M = Fe, Mn; x = 0, 1) Compounds

	B_R	B_V	B	G_R	G_V	G	B/G	E	ν
$LiFePO_4$	94.55	95.41	94.98	45.93	47.50	46.72	2.04	120.41	0.289
ref 51	93.00	94.70	93.90	47.20	49.60	48.40	1.92	123.90	0.280
$FePO_4$	64.85	71.64	68.25	43.36	46.24	44.80	1.52	110.27	0.231
ref 51	72.70	74.50	73.60	50.30	52.50	51.40	1.45	125.00	0.220
$LiMnPO_4$	83.36	83.87	83.62	38.78	40.30	39.54	2.13	102.46	0.296
$MnPO_4$	31.49	32.03	31.76	27.90	41.04	34.47	0.92	75.94	0.102

showed in SI, while the calculated elastic constants of Li_xMPO_4 (M = Fe, Mn; x = 0, 1) compounds are listed in Table 3.

Born and Huang[48] have systematically investigated the lattice mechanical stability and formulated the stability criteria in terms of the elastic constants C_{ij}, and they pointed out that the criterion for a mechanically stable lattice requires that the elastic energy density be a positive definite quadratic function of strain. For orthorhombic crystals, the specific criterions related to the elastic constants (SI) should be further considered.[49,50]

It can be found that the mechanical stability conditions are satisfied for both $LiFePO_4$ and $FePO_4$. Our calculated results are also highly in accordance with the GGA+U values obtained by Maxisch.[51] Usually, C_{11}, C_{22}, and C_{33} measure respectively the a, b, and c directional resistance to the linear compressions, while C_{44}, C_{55}, and C_{66} are related to the shear resistance regarding to the {100}, {010}, and {001} planes, respectively. The values from Table 3 clearly showed that C_{11}, C_{22}, and C_{33} are much larger than C_{44}, C_{55}, and C_{66} in Li_xFePO_4. The result indicated that the resistance of materials against uniaxial tensions is rather strong, while the shear deformations are much easier to occur. When Li^+ is deintercalated from the cathode, C_{22}, C_{33}, C_{12}, and C_{23} decrease obviously while C_{11} increases by about 42.16 GPa in $FePO_4$. This anomaly is also observed by Maxisch et al.,[51] and they proposed that under a compression along a axis, the PO_4 tetrahedrons are slightly rotating while moving towards the unoccupied lithium sites, leading to an increase of C_{11}. Although each C_{ij} value of $LiMnPO_4$ decreases slightly with respect to $LiFePO_4$, its elastic constants show rather similar characteristics, which implies that the bonding features of the two compounds would be analogous. Nevertheless, different from $FePO_4$, Li^+ extraction from $LiMnPO_4$ results in an entirely different set of elastic constants. Except of C_{22} and C_{55}, other C_{ij} values in $MnPO_4$ are all reduced, and C_{12} and C_{23} even turn into negative. Such an abnormality suggested that the bonding characteristics of $MnPO_4$ would be changed significantly.

Despite of the elastic constants, there are still many quantities that can further describe the mechanical properties of a crystal. At present, the cathode materials are usually synthesized as sintered powder, and larger single crystal is barely used in batteries not only because of the preparation difficulties but also because of its poor electrochemical activities. As the sintered powder can be considered as polycrystalline samples aggregated by single phase monocrystals with a random orientation, to obtain a reasonable result, the moduli for polycrystalline materials should be used in the present case. There are two approximation methods to calculate the polycrystalline modulus, namely, the Voigt scheme and the Reuss one. For orthorhombic crystals, the shear modulus (G) and the bulk modulus (B) according to Reuss (G_R and B_R) and Voigt (G_V and B_V) approximations can be calculated in terms of the elastic constants (SI).

It has been proved that the Voigt and Reuss equations represent the upper and lower limits of the true polycrystalline constants.[52] The arithmetic average of the Voigt and the Reuss bounds, which is the best estimation of the theoretical polycrystalline elastic modulus, is called the Voigt−Reuss−Hill (VRH) average,

$$G = \frac{G_R + G_V}{2} \tag{5}$$

$$B = \frac{B_R + B_V}{2} \tag{6}$$

Young modulus (E) and Poisson coefficient (ν) can be further determined by using the following relations:[53]

$$E = \frac{9BG}{3B + G} \tag{7}$$

$$\nu = \frac{3B - 2G}{6B + 2G} \tag{8}$$

Using the relations above, the calculated values are summarized in Table 4. The bulk moduli are a measure of resistance to volume change by an applied pressure, whereas the shear modulus is a measure of resistance to reversible deformations upon shear stress. It can be found that the bulk moduli of $LiFePO_4$, $LiMnPO_4$, and $FePO_4$ are much larger than the corresponding shear moduli, suggesting that they have a higher resistance to volume deformations under isotropic hydrostatic pressure. However, the bulk modulus (31.76 GPa) of $MnPO_4$ is smaller than its shear one (34.47 GPa). It is not difficult to image such an unusual behavior, since the modulus is calculated according to C_{ij}, which have already been discussed above.

dx.doi.org/10.1021/am4054833 | ACS Appl. Mater. Interfaces 2014, 6, 4033−4042

Table 5. Anisotropic Properties of Li_xMPO_4 (M = Fe, Mn; x = 0, 1) Compounds

	A_1	A_2	A_3	$A_{a/b}$	$A_{a/c}$	A_G (%)	A_B (%)
$LiFePO_4$	0.794	0.698	0.958	0.662	0.821	1.68	0.45
ref 51	0.712	0.724	0.995	0.573	0.846	2.44	0.87
$FePO_4$	0.697	0.876	0.728	3.278	2.502	3.21	4.97
ref 51	0.766	0.761	0.822	1.654	1.709	2.11	1.26
$LiMnPO_4$	0.721	0.669	1.079	0.729	0.956	1.92	0.30
$MnPO_4$	0.519	0.747	0.212	0.842	1.087	19.05	0.85

Being of the most importance, the B/G ratio is a relationship empirically linking the plastic and elastic properties of materials.[54] A high B/G ratio is associated with ductility, whereas a low value corresponds to brittleness. The critical value distinguishing the two behaviors was fixed at about 1.75.[55] The ratios for $LiFePO_4$ and $LiMnPO_4$ are 2.04 and 2.13 respectively, and they both have excellent ductility. With Li^+ deintercalation, the value for $FePO_4$ is changed to 1.52, and $FePO_4$ is slightly brittle. However, the value for $MnPO_4$ (0.92) is much lower than 1.75, and it can be anticipated that the crack tip stress will exceed the theoretical tensile stress before the theoretical shear stress was reached. Orthorhombic $MnPO_4$ is thus rather brittle.

Poisson's ratio (ν) measures the stability of a crystal against shear. A smaller (larger) value indicates that the material is relatively stable (unstable) against shear. The Poisson's ratio of $FePO_4$ (0.231) is smaller than those of $LiFePO_4$ (0.289) and $LiMnPO_4$ (0.296), and $FePO_4$ will be more stable under shear situation. Moreover, it is interesting to note that the Poisson's ration of $MnPO_4$ (only 0.102) is very small, which implies that $MnPO_4$ would be rather stable against shear. However, in consideration of the definition of this quantity (eq 8), it can be found that the Poisson's ratio depends heavily on the difference between bulk and shear modulus. The very close bulk and shear modulus of $MnPO_4$ is thus responsible for the smallest calculated Poisson's ratio. As the shear modulus of $MnPO_4$ is too small, such an intrinsic shortcoming can still make the shear deformation happen easily. Together with its brittle feature, it can be expected that the volume change of $MnPO_4$ with respect to $LiMnPO_4$ is very large.

It is well known that the induced micro cracks in ceramics are due to the anisotropic thermal expansion coefficient as well as the elastic anisotropy.[55,56] Especially in lithium ion batteries, repeated insertion/extraction of Li^+ will change the elastic anisotropy of the cathode materials, leading to the micro cracks and capacity fade of batteries. For orthorhombic materials, elastic anisotropy arises from two aspects, the shear anisotropy and linear bulk modulus anisotropy. The first one provides a measure of the anisotropy degree in the bonding between atoms in different planes. In cubic system, the shear anisotropy is sufficient to describe the elastic anisotropy, because the latter one is the same for all directions. The shear anisotropic factor for the {100} shear planes between the ⟨011⟩ and ⟨010⟩ directions is[55]

$$A_1 = \frac{4C_{44}}{C_{11} + C_{33} - 2C_{13}} \tag{9}$$

For the {010} shear planes between the ⟨101⟩ and ⟨001⟩ direction, it is

$$A_2 = \frac{4C_{55}}{C_{22} + C_{33} - 2C_{23}} \tag{10}$$

For the {001} shear planes between the ⟨110⟩ and ⟨010⟩ direction, it is

$$A_3 = \frac{4C_{66}}{C_{11} + C_{22} - 2C_{12}} \tag{11}$$

The obtained shear anisotropic factors are given in Table 5.

For an isotropic crystal, A_1, A_2, and A_3 must be one, while any values deviated from 1 corresponds to a certain degree of elastic anisotropy. For $LiFePO_4$, A_3 (0.958) is very close to 1, whereas A_2 is (0.698) a little bit smaller than 1. The results indicated that the atomic bonding in the {001} planes shows isotropic characteristics, and it is anisotropic in the {010} planes. After Li^+ extraction, A_1 and A_3 are reduced, while A_2 increase, suggesting significant anisotropy changes in Li_xFePO_4. Moreover, it can be found that the deviations of A_1, A_2, and A_3 in $LiMnPO_4$ are slightly larger than those in $LiFePO_4$, and the atomic bonding in {100}, {010}, and {001} planes is more anisotropic in $LiMnPO_4$. For $MnPO_4$, A_1 (0.519) and A_3 (0.212) are abnormally small. Therefore, the atomic bonding of $MnPO_4$ concerning the {100} and {001} planes will undergo drastic changes to display strong anisotropic properties, which deserves our further considerations.

To investigate the linear bulk modulus anisotropy, we have calculated the bulk modulus along the crystal axis, defined as $B_a = a(\mathrm{d}P/\mathrm{d}a)$, $B_b = b(\mathrm{d}P/\mathrm{d}b)$, and $B_c = c(\mathrm{d}P/\mathrm{d}c)$.[55] The anisotropy of the bulk modulus along a axis with respect to b and c axes can be written as $A_{a/b} = (B_a/B_b)$ and $A_{a/c} = (B_a/B_c)$. Like the shear anisotropy, a value of 1 indicates isotropy, while any values deviated from 1 correspond to a certain degree of anisotropy. For Li_xFePO_4, $A_{a/b}$ and $A_{a/c}$ are changed from 0.662 and 0.821 to 3.278 and 2.502 respectively, indicating linear bulk modulus anisotropy exists in the compounds. For Li_xMnPO_4, their anisotropies of the linear bulk modulus are smaller than those of Li_xFePO_4, since the relevant values are more close to 1. Although the above quantities provide some useful information on the elastic anisotropy of compounds, the analysis is still quite qualitative. To provide a more practical concept on the anisotropy in percentage, we applied the definition proposed by Chung and Buessem[57]

$$A_B = \frac{B_V - B_R}{B_V + B_R} \tag{12}$$

$$A_G = \frac{G_V - G_R}{G_V + G_R} \tag{13}$$

where B and G are the bulk and shear moduli, and the subscripts V and R represent the Voigt and Reuss bounds. For these two expressions, a value of zero represents elastic isotropy and a value of 100% is the largest possible anisotropy. The results clearly showed that the elastic anisotropy caused by the shear component is much larger than that by linear bulk counterpart in $LiFePO_4$ and $LiMnPO_4$. After Li^+ extraction, the

anisotropy from shear and linear bulk modulus increases obvious in $FePO_4$, and A_B becomes even larger than A_G. However, the situation in $MnPO_4$ is entirely different. The A_B value for $MnPO_4$ is 0.85%, while A_G has already reached 19.05%. Therefore, in $MnPO_4$ compound, the elastic anisotropy is mainly originated from the shear component. The very larger shear anisotropy in $MnPO_4$ will make the micro cracks and dislocations very easy to occur during the charging and discharging process, leading to performance degeneration of the batteries. It should be emphasized that the abnormal A_G is connected to A_1 and A_3 (or C_{44} and C_{66}). More specifically, such an abnormality is also related to the anisotropic bonding characteristics of the compounds at certain crystal planes.

Because the macroscopic mechanical properties are representations of microscopic bonding, to bridge the relationship between them, the electronic structures should be investigated in detail, which will be discussed below.

3.3. Microscopic Bonding of $LiMPO_4$ and MPO_4 (M = Fe, Mn) Compounds. It is certain that the high spin arrangement of Mn ions in MnO_6 octahedrons of the compounds does result in a very large Jahn-Teller distortion. This phenomenon is well known and approved by many literatures of $LiMn_2O_4$,[58] Li_2MnSiO_4,[59] and $LiMnPO_4$.[30] After analyzing the bonding characteristics, we found pronounced differences between the Li_xFePO_4 and Li_xMnPO_4. For $LiFePO_4$, Li^+ deintercalation leads to shorter Fe−O(I) and longer Fe−O(II) bonds as given in Table 6, and the two kinds

Table 6. M−O Bond Length (in Å) for Li_xMPO_4 (M = Fe, Mn; x = 0, 1) Compounds

	M−O(I)	M−O(II)	M−O(III)	M−O(I)/M−O(II)[b]
$LiFePO_4$	2.258	2.062	2.159	1.095
$FePO_4$	2.176	2.106	1.922	1.033
Δ (in %)[a]	−3.63	2.13	−10.98	
$LiMnPO_4$	2.307	2.162	2.225	1.067
$MnPO_4$	2.365	2.028	1.923	1.166
Δ (in %)[a]	2.51	−6.19	−13.57	

[a]Positive and negative values mean compression and expansion, respectively. [b]An indicator for evaluating the distortion of the MO_6 octahedron equatorial planes.

of bonds trend to be equal. This result means that the distortions of FeO_6 octahedrons within the equatorial plane will diminish. On the contrary, Mn−O(I) and Mn−O(II) bonds display an opposite trend in Li_xMnPO_4 systems. For $MnPO_4$, the Mn−O(I)/Mn−O(II) ratio has reached 1.166, the largest value among the investigated models. More importantly, because of the structural changes, the spatial charge distributions would be entirely different.

As confirmed by Table 6 and Figure 3, M−O(I) bonds are much weaker than other covalent bonds. For a covalent crystal, weaker chemical bonds will lead to two consequences. The first one is that the bonds are easier to break or cleave, which is related to the brittle characteristics of the crystals. Second, weaker bonds will make some slip systems become active and the shear deformations at certain direction are easier, which is related to the ductile properties of the crystals. The two behaviors compete and cooperate to determine the overall mechanical properties of the crystals. Our calculation suggested that the very weak M−O(I) bonds are responsible for the small C_{44} and C_{66}, while the M-O(II) bonds lead to a small C_{55} (SI). Moreover, it is interesting to note that the weak M−O(I)

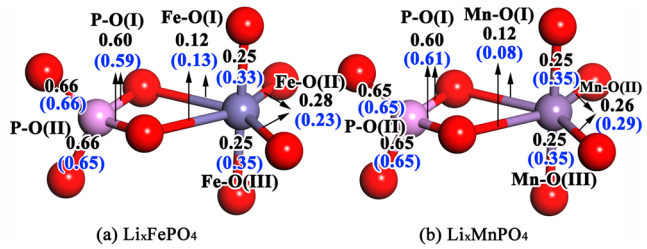

Figure 3. Mulliken overlap populations (bond orders) for (a) Li_xFePO_4 and (b) Li_xMnPO_4 (x = 0, 1). Black values are for $LiMPO_4$ materials, while blue ones in parentheses for MPO_4. In $LiMPO_4$ compounds, the Li−O bond populations are calculated to be about 0.01, which means pure ionic bonds.

bonds are further weakened by about 33% (0.08) in $MnPO_4$, which is opposite to the Li_xFePO_4 case. If the crystal orientation is taken into account, it can be identified that the Mn−O(I) bonds are mainly spread within the {101} and {$\bar{1}$01} crystal planes, as depicted in Fig. 4.

Therefore, the slip systems concerning these two crystal plane family (parallel to y axis), that is, ⟨010⟩{101},⟨10$\bar{1}$⟩{101}, ⟨010⟩{$\bar{1}$01}, and ⟨101⟩{$\bar{1}$01} ones, will become very active in $MnPO_4$, which well explains why C_{55} (yy, 48.71 GPa) can still retain a relative larger value while C_{44} (xx, 16.96 GPa) and C_{66} (zz, 17.93 GPa) decrease obviously with respect to $LiMnPO_4$. It should be emphasized that the very weak Mn−O(I) bonds in $MnPO_4$ also play an important role in the linear compressions along the [100] and [001] directions. As can be confirmed from Table 3, C_{11} and C_{33} are abnormally reduced, and C_{12} and C_{23} even become negative after Li^+ deintercalation. The bulk modulus of $MnPO_4$ thus significantly decreases, making the material very brittle as suggested above.

Owning to the very active slip systems in $MnPO_4$, the shear deformation and dislocation will occur easily. As illustrated in Fig.4, the dislocations along (101) and ($\bar{1}$01) planes allow two adjacent MnO_6 octahedrons form a shared edge, and the two nearest PO_4 tetrahedrons are connected through one shared oxygen vertex. One redundant O atom per $Mn_2P_2O_8$ unit will be release at the interface. Therefore, the chemical reaction[60]

$$2MnPO_4 \underset{Pnma}{\rightarrow} Mn_2P_2O_7 \underset{C2/m}{} + 0.5O_2$$

become possible, although this decomposition reaction is found to be endothermic. The result is highly coincident with the observed phase transformation. As a result, the mechanical reason will play an important role for the poor cycling stability of $MnPO_4$, which makes $MnPO_4$ entirely different from $FePO_4$.

4. CONCLUSION

Relying on first-principles technique, we have investigated the thermodynamic stabilities of two representative olivine-type $LiMPO_4$ compounds. The results identified that Li_xFePO_4 and Li_xMnPO_4 have comparable thermal stability in their lithiated/delithiated states, and they are also much more stable with respect to the relevant oxides than some other classic cathode materials ($LiNiO_2$, $LiCoO_2$, etc.). However, the relatively good thermodynamic stability of $MnPO_4$ cannot guarantee the absence of the well known phase transformation from $MnPO_4$ to $Mn_2P_2O_7$. To reveal the microscopic origin and driving force, systematical investigation on the mechanical properties of the compounds is performed. It is found that the M−O(I) bonds are much weaker than other covalent bonds,

dx.doi.org/10.1021/am4054833 | ACS Appl. Mater. Interfaces 2014, 6, 4033−4042

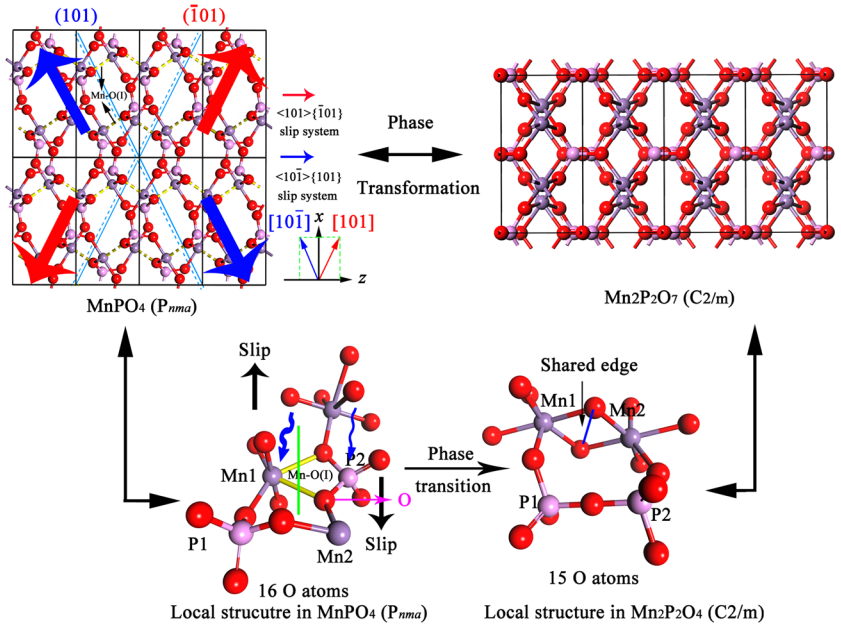

Figure 4. Phase transformation mechanism for $MnPO_4$ compound. [010] direction (*y* axis or *yy* in the Voigt notation) is perpendicular to the paper.

and this feature can be associated with the relative small C_{44} and C_{66} of Li_xMPO_4 compounds. While M−O(II) bonds are responsible for the small C_{55}. Because Li^+ deintercalation further weakens the Mn−O(I) bonds, $MnPO_4$ thus becomes very brittle. Moreover, the anisotropic properties of the compounds, which usually relate to the micro cracks of materials, are also discussed. The elastic anisotropy of $MnPO_4$ is abnormally large and mainly originated from the shear component (A_G, 19.05%), which indicates that the shear deformation and dislocation in $MnPO_4$ are very easy to occur. Therefore, the phase transformation in $MnPO_4$ will appear. As the unusually mechanical properties of $MnPO_4$ are dominant by the Mn−O(I) bonds spread within the {101} and {1̄01} crystal planes, it can be deduced that the mechanical factor will play an important role for the phase transformation of $MnPO_4$, which makes $MnPO_4$ different from $FePO_4$. The present applied method can be useful to better predict an intricate relationship between the electrochemical performance and the structure configuration, and it will contribute to the development of safe and stable new type electrode materials.

■ ASSOCIATED CONTENT

Supporting Information

Algorithms for calculating the Gibbs free energies and mechanical properties and correlation between shear deformation and chemical bonds. This information is available free of charge via the Internet at http://pubs.acs.org/.

■ AUTHOR INFORMATION

Corresponding Authors

*E-mail: xieying@hlju.edu.cn.
*E-mail: tfyihit@163.com. Tel.: +86-555 2311807. Fax: +86 555 2311552.

Notes

The authors declare no competing financial interest.

■ ACKNOWLEDGMENTS

This work was financially supported by the National Natural Science Foundation of China (nos. 21301052, 51274002 and 21173072), the Natural Science Foundation of Heilongjiang Province (no. B201003), the Opening Project of Key Laboratory of Functional Inorganic Material Chemistry (Heilongjiang University, Ministry of Education), the Specialized Research Fund for the Doctoral Program of Higher Education (no. 20132301120001), and the Program for Innovative Research Team in Anhui University of Technology (no. TD201202).

■ REFERENCES

(1) Ji, L.; Lin, Z.; Alcoutlabi, M.; Zhang, X. Recent Developments in Nanostructured Anode Materials for Rechargeable Lithium-ion Batteries. *Energy Environ. Sci.* **2011**, *4*, 2682−2699.
(2) Zhou, X.; Tang, J.; Yang, J.; Xie, J.; Huang, B. Seaweed-like Porous Carbon from the Decomposition of Polypyrrole Nanowires for Application in Lithium Ion Batteries. *J. Mater. Chem. A* **2013**, *1*, 5037−5044.
(3) Zhou, X.; Ma, L.; Yang, J.; Huang, B.; Zou, Y.; Tang, J.; Xie, J.; Wang, S.; Chen, G. Properties of Graphitized Boron-Doped Coal-Based Coke Powders as Anode for Lithium-Ion Batteries. *J. Electroanal. Chem.* **2013**, *698*, 39−44.
(4) Armand, M.; Tarascon, J.-M. Building Better Batteries. *Nature* **2008**, *451*, 652−657.
(5) Barpanda, P.; Ati, M.; Melot, B. C.; Rousse, G.; Chotard, J.-N.; Doublet, M.-L.; Sougrati, M. T.; S. Corr, A.; Jumas, J.-C.; Tarascon, J.-M. A 3.90 V Iron-Based Fluorosulphate Material for Lithium-Ion Batteries Crystallizing in the Triplite Structure. *Nat. Mater.* **2011**, *10*, 772−779.
(6) Toprakci, O.; Ji, L.; Lin, Z.; Toprakci, H. A. K.; Zhang, X. Fabrication and Electrochemical Characteristics of Electrospun $LiFePO_4$/Carbon Composite Fibers for Lithium-ion batteries. *J. Power Sources* **2011**, *196*, 7692−7699.
(7) Bakenov, Z.; Taniguchi, I. Physical and Electrochemical Properties of $LiMnPO_4$/C Composite Cathode Prepared with Different Conductive Carbons. *J. Power Sources* **2010**, *195*, 7445−7451.
(8) Theil, S.; Fleischhammer, M.; Axmann, P.; Wohlfahrt-Mehrens, M. Experimental Investigations on the Electrochemical and Thermal

Behaviour of $LiCoPO_4$-Based Cathode. *J. Power Sources* **2013**, *222*, 72−78.
(9) Minakshi, M.; Singh, P.; Appadoo, D.; Martin, D. E. Synthesis and Characterization of Olivine $LiNiPO_4$ for Aqueous Rechargeable Battery. *Electrochim. Acta* **2011**, *56*, 4356−4360.
(10) Wolfenstine, J.; Allen, J. $LiNiPO_4$−$LiCoPO_4$ Solid Solutions as Cathodes. *J. Power Sources* **2004**, *136*, 150−153.
(11) Wolfenstine, J.; Allen, J. Ni^{3+}/Ni^{2+} Redox Potential in $LiNiPO_4$. *J. Power Sources* **2005**, *142*, 389−390.
(12) Devaraju, M. K.; Honma, I. Hydrothermal and Solvothermal Process Towards Development of $LiMPO_4$ (M = Fe, Mn) Nanomaterials for Lithium-Ion Batteries. *Adv. Energy Mater.* **2012**, *2*, 284−297.
(13) Chen, Z.; Dahn, J. R. Reducing Carbon in $LiFePO_4$ / C Composite Electrodes to Maximize Specific Energy, Volumetric Energy, and Tap Density. *J. Electrochem. Soc.* **2002**, *149*, A1184−A1189.
(14) Kobayashi, G.; Nishimura, S.-i.; Park, M.-S.; Kanno, R.; Yashima, M.; Ida, T.; Yamada, A. Isolation of Solid Solution Phases in Size-Controlled Li_xFePO_4 at Room Temperature. *Adv. Funct. Mater.* **2009**, *19*, 395−403.
(15) Zhang, W.-J. Structure and Performance of $LiFePO_4$ Cathode Materials: A Review. *J. Power Sources* **2011**, *196*, 2962−2970.
(16) Delacourt, C.; Laffont, L.; Bouchet, R.; Wurm, C.; Leriche, J. B.; Morcrette, M.; Tarascon, J. M.; Masquelier, C. Toward Understanding of Electrical Limitations (Electronic, Ionic) in $LiMPO_4$ (M = Fe, Mn) Electrode Materials. *J. Electrochem. Soc.* **2005**, *152*, A913−A921.
(17) Chen, G. Y.; Wilcox, J. D.; Richardson, T. J. Improving the Performance of Lithium Manganese Phosphate Through Divalent Cation Substitution. *Electrochem. Solid-State Lett.* **2008**, *11*, A190−A194.
(18) Mishima, Yu.; Hojo, T.; Nishio, T.; Sadamura, H.; Oyama, N.; Moriyoshi, C.; Kuroiwa, Y. MEM Charge Density Study of Olivine $LiMPO_4$ and MPO_4 (M = Mn, Fe) as Cathode Materials for Lithium-Ion Batteries. *J. Phys. Chem. C* **2013**, *117*, 2608−2615.
(19) Meethong, N.; Huang, H. Y. S.; Speakman, S. A.; Carter, W. C.; Chiang, Y. M. Strain Accommodation during Phase Transformations in Olivine-Based Cathodes as a Materials Selection Criterion for High-Power Rechargeable Batteries. *Adv. Funct. Mater.* **2007**, *17*, 1115−1123.
(20) Meng, Y. S.; Arroyo-de Dompablo, M. E. First Principles Computational Materials Design for Energy Storage Materials in Lithium Ion Batteries. *Energy Environ. Sci.* **2009**, *2*, 589−609.
(21) Ceder, G. Opportunities and Challenges for First-Principles Materials Design and Applications to Li Battery Materials. *MRS Bull.* **2010**, *35*, 693−701.
(22) Yoshida, J.; Nakanishi, S.; Iba, H. Thermal Behavior of Delithiated $Li_{1-x}MnPO_4$ ($0 \leq x < 1$) Structure for Lithium-Ion Batteries. *Int. J. Appl. Ceram. Technol.* **2013**, *10*, 764−772.
(23) Aravindan, V.; Gnanaraj, J.; Lee, Y.-S.; Madhavi, S. $LiMnPO_4$—A Next Generation Cathode Material for Lithium-Ion Batteries. *J. Mater. Chem. A* **2013**, *1*, 3518−3539.
(24) Segall, M.D.; Lindan, P.J.D.; Probert, M.J.; Pickard, C.J.; Hasnip, P.J.; Clark, S.J.; Payne, M.C. First-Principles Simulation: Ideas, Illustrations and the CASTEP Code. *J. Phys.: Condens. Matter* **2002**, *14*, 2717−2744.
(25) Perdew, J.P.; Wang, Y. Accurate and Simple Analytic Representation of the Electron−Gas Correlation Energy. *Phys. Rev. B* **1992**, *45*, 13244−13249.
(26) Monkhorst, H. J.; Pack, J. D. Special Points for Brillouin-Zone Integrations. *Phys. Rev. B* **1976**, *13*, 5188−5192.
(27) Fischer, T.H.; Almlof, J. General Methods for Geometry and Wave Function Optimization. *J. Phys. Chem.* **1992**, *96*, 9768−9774.
(28) Yonemura, M.; Yamada, A.; Takei, Y.; Sonoyama, N.; Kanno, R. Comparative Kinetic Study of Olivine Li_xMPO_4 (M = Fe, Mn). *J. Electrochem. Soc.* **2004**, *151*, A1352−A1356.
(29) Andersson, A. S.; Kalska, B.; Häggström, L.; Thomas, J. O. Lithium Extraction/insertion in $LiFePO_4$: An X-ray Diffraction and Mössbauer Spectroscopy Study. *Solid State Ionics* **2000**, *130*, 41−52.
(30) Dong, Y.; Wang, L.; Zhang, S.; Zhao, Y.; Zhou, J.; Xie, H.; Goodenough, J. B. Two-Phase Interface in $LiMnPO_4$ Nanoplates. *J. Power Sources* **2012**, *215*, 116−121.
(31) Gong, Z.; Yang, Y. Recent Advances in the Research of Polyanion-type Cathode Materials for Li-Ion Batteries. *Energy Environ. Sci.* **2011**, *4*, 3223−3242.
(32) Meethong, N.; Kao, Y. H.; Tang, M.; Huang, H. Y.; Carter, W. C.; Chiang, Y. M. Electrochemically Induced Phase Transformation in Nanoscale Olivines $Li_{1-x}MPO_4$ (M = Fe, Mn). *Chem. Mater.* **2008**, *20*, 6189−6198.
(33) Aydinol, M.; Kohan, A.; Ceder, G. Ab initio Study of Lithium Intercalation in Metal Oxides and Metal Dichalcogenides. *Phys. Rev. B* **1997**, *56*, 1354−1365.
(34) Islam, M. S.; Davies, R. A.; Gale, J. D. Structural and Electronic Properties of the Layered $LiNi_{0.5}Mn_{0.5}O_2$ Lithium Battery Material. *Chem. Mater.* **2003**, *15*, 4280−4286.
(35) Barin, I. *Thermochemical Data of Pure Substances*, 3rd ed.; Wiley-VCH Verlag GmbH: Weinheim, Germany, 1995.
(36) Wang, Y.; Wang, Y.; Hosono, E.; Wang, K.; Zhou, H. The Design of a $LiFePO_4$/Carbon Nanocomposite with a Core−Shell Structure and Its Synthesis by an In Situ Polymerization Restriction Method. *Angew. Chem., Int. Ed.* **2008**, *47*, 7461−7465.
(37) Kang, B.; Ceder, G. Electrochemical Performance of $LiMnPO_4$ Synthesized with Off-Stoichiometry. *J. Electrochem. Soc.* **2010**, *157*, A808−A811.
(38) Choi, D.; Xiao, J.; Choi, Y. J.; Hardy, J. S.; Vijayakumar, M.; Bhuvaneswari, M. S.; Liu, J.; Xu, W.; Wang, W.; Yang, Z.; Graff, G. L.; Zhang, J.-G. Thermal Stability and Phase Transformation of Electrochemically Charged/discharged $LiMnPO_4$ Cathode for Li-Ion Batteries. *Energy Environ. Sci.* **2011**, *4*, 4560−4566.
(39) Wang, M.; Navrotsky, A. $LiMO_2$ (M = Mn, Fe, and Co): Energetics, Polymorphism and Phase Transformation. *J. Solid State Chem* **2005**, *178*, 1230−1240.
(40) Wang, M.; Navrotsky, A. Enthalpy of Formation of $LiNiO_2$, $LiCoO_2$, and Their Solid Solution, $LiNi_{1-x}Co_xO_2$. *Solid State Ionics* **2004**, *166*, 167−173.
(41) Wang, M.; Navrotsky, A. Thermochemistry of $Li_{1+x}Mn_{2-x}O_4$ ($0 \leq x \leq 1/3$) Spinel. *J. Solid State Chem.* **2005**, *178*, 1182−1189.
(42) Ong, S. P.; Mo, Y. F.; Richards, W. D.; Lee, H. S.; Ceder, G. Phase Stability, Electrochemical Stability and Ionic Conductivity of the $Li_{10\pm1}MP_2X_{12}$ (M = Ge, Si, Sn, Al, or P, and X = O, S, or Se) Family of Superionic Conductors. *Energy Environ. Sci.* **2013**, *6*, 148−156.
(43) Ong, S. P.; Wang, L.; Kang, B.; Ceder, G. Li−Fe−P−O_2 Phase Diagram from First Principles Calculations. *Chem. Mater.* **2008**, *20*, 1798−1807.
(44) Fey, G. T.-K.; Muralidharan, P.; Lu, C.-Z.; Cho, Y.-D. Enhanced Electrochemical Performance and Thermal Stability of La_2O_3-Coated $LiCoO_2$. *Electrochim. Acta* **2006**, *51*, 4850−4858.
(45) Delacourt, C.; Poizot, P.; Tarascon, J.-M.; Masquelier, C. The Existence of a Temperature-Driven Solid Solution in Li_xFePO_4 for $0 \leq x \leq 1$. *Nat. Mater.* **2005**, *4*, 254−260.
(46) Ong, S. P.; Jain, A.; Hautier, G.; Kang, B.; Ceder, G. Thermal Stabilities of Delithiated Olivine MPO_4 (M = Fe, Mn) Cathodes Investigated Using First Principles Calculations. *Electrochem. Commun.* **2010**, *12*, 427−430.
(47) Martha, S.K.; Haik, O.; Zinigrad, E.; Exnar, I.; Drezen, T.; Miners, J. H.; Aurbacha, D. On the Thermal Stability of Olivine Cathode Materials for Lithium-Ion Batteries. *J. Electrochem.Soc.* **2011**, *158*, A1115−A1122.
(48) Born, M.; Huang, K. *Dynamical Theory of Crystal Lattices*; Oxford University Press: Oxford, U.K.,1998.
(49) Jiang, C.; Srinivasan, S. G.; Caro, A.; Maloy, S. A. Structural, Elastic, and Electronic Properties of Fe_3C from First Principles. *J. Appl. Phys.* **2008**, *103*, No. 043502.
(50) Koc, H.; Mamedov, A. M.; Deligoz, E.; Ozisik, H. First Principles Prediction of the Elastic, Electronic, and Optical Properties of Sb_2S_3 and Sb_2Se_3 Compounds. *Solid State Sci.* **2012**, *14*, 1211−1220.
(51) Maxisch, T.; Ceder, G. Elastic Properties of Olivine Li_xFePO_4 from First Principles. *Phys. Rev. B* **2006**, *73*, No. 174112.

(52) Hill, R. The Elastic Behaviour of a Crystalline Aggregate. *Proc. Phys. Soc. London Sect. A* **1952**, *65*, 349−354.
(53) Caravaca, M. A.; Mino, J. C.; Pérez, V. J.; Casali, R. A.; Ponce, C. A. Ab Initio Study of the Elastic Properties of Single and Polycrystal TiO_2, ZrO_2 and HfO_2 in the Cotunnite Structure. *J. Phys.: Condens. Matter* **2009**, *21*, No. 015501.
(54) Pugh, S. F. Relations between the Elastic Moduli and the Plastic Properties of Polycrystalline Pure Metals. *Philos. Mag.* **1954**, *45*, 823−843.
(55) Ravindran, P.; Fast, L.; Korzhavyi, P. A.; Johansson, B.; Wills, J.; Eriksson, O. Density Functional Theory for Calculation of Elastic Properties of Orthorhombic Crystals: Application to $TiSi_2$. *J. Appl. Phys.* **1998**, *84*, 4891−4904.
(56) Tvergaard, V.; Hutchinson, J. W. Microcracking in Ceramics Induced by Thermal Expansion or Elastic Anisotropy. *J. Am. Ceram. Soc.* **1988**, *71*, 157−166.
(57) Chung, D. H.; Buessem, W. R. In *Anisotropy in Single Crystal Refractory Compound*; Vahldiek, F. W., Mersol, S. A., eds.; Plenum: New York, 1968; Vol. 2, p 217.
(58) Yamada, A.; Tanaka, M.; Tanaka, K.; Sekai, K. Jahn−Teller Instability in Spinel Li−Mn−O. *J. Power Sources* **1999**, *81-82*, 73−78.
(59) Xu, B.; Qian, D.; Wang, Z.; Meng, Y. S. Recent Progress in Cathode Materials Research for Advanced Lithium Ion Batteries. *Mater. Sci. Eng. R-Rep.* **2012**, *73*, 51−65.
(60) Kim, S.-W.; Kim, J.; Gwon, H.; Kang, K. Phase Stability Study of $Li_{1-x}MnPO_4$ ($0 \leq x \leq 1$) Cathode for Li Rechargeable Battery. *J. Electrochem. Soc.* **2009**, *156*, A635−A638.